Reduction of Chlorinated Ethanes by Nanosized Zero-Valent Iron: Kinetics, Pathways, and Effects of Reaction Conditions

ARTICLE *in* ENVIRONMENTAL SCIENCE AND TECHNOLOGY · AUGUST 2005

Impact Factor: 5.33 · DOI: 10.1021/es048262e · Source: PubMed

2 AUTHORS:

Hocheol Song
Sejong University
61 PUBLICATIONS **1,141** CITATIONS
SEE PROFILE

Elizabeth Carraway
Clemson University
46 PUBLICATIONS **2,318** CITATIONS
SEE PROFILE

Environ. Sci. Technol. **2005**, *39,* 6237−6245

Reduction of Chlorinated Ethanes by Nanosized Zero-Valent Iron: Kinetics, Pathways, and Effects of Reaction Conditions

HOCHEOL SONG AND
ELIZABETH R. CARRAWAY*
Department of Environmental Engineering and Science, Clemson University, 342 Computer Court, Anderson, South Carolina 29625

Nanosized iron (<100 nm in diameter) was synthesized in the laboratory and applied to the reduction of eight chlorinated ethanes (hexachloroethane (HCA), pentachloroethane (PCA), 1,1,2,2-tetrachloroethane (1,1,2,2-TeCA), 1,1,1,2-tetrachloroethane (1,1,1,2-TeCA), 1,1,2-trichloroethane (1,1,2-TCA), 1,1,1-trichloroethane (1,1,1-TCA), 1,2-dichloroethane (1,2-DCA), and 1,1-dichloroethane (1,1-DCA)) in batch reactors. Reduction of 1,1,1-TCA increased linearly with increasing iron loading between 0.01 and 0.05 g per 124 mL solution (0.08−0.4 g/L). Varying initial concentrations of PCA between 0.025 and 0.125 mM resulted in relatively constant pseudo-first-order rate constants, indicating PCA removal conforms to pseudo-first-order kinetics. The reduction of 1,1,2,2-TeCA decreased with increasing pH; however, dehydrohalogenation of 1,1,2,2-TeCA became important at high pH. All chlorinated ethanes except 1,2-DCA were transformed to less chlorinated ethanes or ethenes. The surface-area-normalized rate constants from first-order kinetics analysis ranged from $<4 \times 10^{-6}$ to 0.80 L m^{-2} h^{-1}. In general, the reactivity increased with increasing chlorination. Among tri- and tetrasubstituted compounds, the reactivity was higher for compounds with chlorine atoms more localized on a single carbon (e.g., 1,1,1-TCA > 1,1,2-TCA). Reductive β-elimination was the major pathway for the chlorinated ethanes possessing α,β-pairs of chlorine atoms to form chlorinated ethenes, which subsequently reacted with nanosized iron. Reductive α-elimination and hydrogenolysis were concurrent pathways for compounds possessing chlorine substitution on one carbon only, forming less chlorinated ethanes.

Introduction

Chlorinated ethanes, along with chlorinated ethenes, are a major group of pollutants found in contaminated groundwater (*1*). Some chlorinated ethanes are known or suspected human carcinogens and tend to persist in the environment over an extended period of time due to their inertness to biotic or abiotic transformation reactions. Among the nine species that belong to this group of compounds, five compounds (hexachloroethane (HCA), 1,1,2,2-tetrachloroethane (1,1,2,2-TeCA), 1,1,1,2-tetrachloroethane (1,1,1,2-TeCA), 1,1,2-trichloroethane (1,1,2-TCA), and 1,2-dichloroethane (1,2-DCA)) are classified as possible or probable human carcinogens (*2*), and they are generally persistent under typical environmental conditions because of their structural stability and relatively low reduction potentials (~ −0.68 to +0.15 V) (*3*).

While several observations have been reported for biotic (*4*−*6*) or abiotic (*7*−*9*) transformations of chlorinated ethanes, the rate and extent of transformations are highly variable. Under controlled environmental conditions, the type and rate of transformation of chlorinated ethanes have been shown to be dependent on the extent and position of chlorination of the molecule. For example, reductive β-elimination has been shown to be a preferential pathway for compounds possessing α,β-pairs of chlorine atoms (*6*, *10*−*12*), while hydrogenolysis or reductive α-elimination is the primary transformation pathway for compounds possessing only α-chlorines (*11*, *13*, *14*). In addition, dehydrohalogenation becomes important under basic conditions (*7*, *8*). When transformations of chlorinated ethanes occur via β-elimination or dehydrohalogenation, the products formed include chlorinated ethenes. Via hydrogenolysis or α-elimination, chlorinated ethanes with fewer chlorine atoms are produced.

Reactions between zero-valent iron and chlorinated ethanes have received relatively little attention compared to other chlorinated aliphatic compounds, which is surprising considering the widespread occurrence of chlorinated ethanes as groundwater pollutants. Chlorinated ethanes reported to be transformed by iron metal include HCA (*15*, *16*), 1,1,1,2- and 1,1,2,2-TeCA isomers (*15*−*17*), 1,1,1-trichloroethane (1,1,1-TCA) (*13*, *15*, *16*, *18*), and 1,1-dichloroethane (1,1-DCA) (*13*). One report presented disappearance kinetics for four chlorinated ethanes (HCA, 1,1,1,2- and 1,1,2,2-TeCA, and 1,1,1-TCA) (*15*), and another analyzed disappearance kinetics for these four compounds obtained from three experimental studies (*16*). To date, these are the broadest studies of reduction of chlorinated ethanes by zero-valent iron.

The objective of this study was to demonstrate the performance of a laboratory-synthesized nanosized iron in dechlorinating chlorinated ethanes. As a chemical reactant, nanosized iron exhibits high reactivity and high mobility. Nanosized iron has recently been applied to treat various types of environmental contaminants and was proven to be an effective reductant for chlorinated ethenes (*19*−*23*), chlorinated methanes (*24*−*26*), chlorinated benzenes (*19*, *27*), chromium and lead (*28*, *29*), and nitrate (*30*).

Experiments were conducted to study the effects of physicochemical factors including pH, metal loading, and initial concentration on the reduction of selected chlorinated ethanes. Also, all chlorinated ethanes except chloroethane were reacted with nanosized iron to provide detailed data describing the kinetic behavior of parent compounds as well as intermediate and final products. Finally, linear free energy relationships (LFERs) using one-electron reduction potentials (E1) and lowest unoccupied molecular orbital (LUMO) energies as descriptors are presented.

Experimental Section

Materials. Chemicals used in this study were $FeCl_3 \cdot 6H_2O$ (98%, Aldrich), $NaBH_4$ (98%, Aldrich), HCA (99%, Aldrich), PCA (99.4%, Chemservice), 1,1,1,2-TeCA (99%, Aldrich), 1,1,2,2-TeCA (98%, Aldrich), 1,1,1-TCA (99.5%, Chemservice), 1,1,2-TCA (99.5%, Chemservice), 1,1-DCA (99.5%, Chemservice), 1,2-DCA (99.8%, Aldrich), methanol (99.9%, HPLC grade, Burdick & Jackson), pentane (99.9%, GC grade, Burdick & Jackson), and toluene (99.9%, HPLC grade, Burdick &

* Corresponding author phone (864)656-5574; fax: (864)656-0672; e-mail: ecarraw@clemson.edu.

10.1021/es048262e CCC: $30.25
Published on Web 07/14/2005

Jackson). Chemicals used to prepare external calibration curves for reaction product analyses were tetrachloroethene (PCE, 99.9%, HPLC grade, Sigma), trichloroethene (TCE, 99.9%, HPLC grade, Sigma), *cis*-1,2-dichloroethene (*cis*-DCE, 99%, HPLC grade, Sigma), *trans*-1,2-dichloroethene (*trans*-DCE, 99.9%, HPLC grade, Sigma), 1,1-dichloroethene (1,1-DCE, 99.9%, HPLC grade, Sigma), vinyl chloride (VC, 2000 μg/mL in methanol, Chemservice), ethene (1000 ppm and 1% in He, Scott Specialty Gas), and ethane (1000 ppm in He, Scott Specialty Gas). Buffers used were 2-(*N*-morpholino)-ethanesulfonic acid (MES, Sigma), 3-(*N*-morpholino)propanesulfonic acid (MOPS, Sigma), *N*-(2-hydroxyethyl)-piperazine-*N*′-(2-ethanesulfonic acid) (HEPES, Sigma), and *N*-(tris(hydroxymethyl)methyl)-3-aminopropanesulfonic acid (TAPS, Sigma). All chemicals were used as received. Methanolic stock solutions of chlorinated ethanes were prepared from the pure compounds and used within 1 day. Deionized water from a Milli-Q water system (~18 MΩ cm) was deoxygenated by purging with high-purity N_2.

Synthesis of Nanosized Iron. Nanosized iron was synthesized by reduction of ferric chloride (1.2 M, 50 mL) by sodium borohydride (3.6 M, 50 mL), following Glavee et al. (*31*) except that an inert atmosphere (N_2) was maintained throughout the synthesis. Iron was washed with water three times, followed by acetone washing. Dried particles were stored in an anaerobic chamber (5% H_2 in N_2 atmosphere, Coy) to avoid air contact. If contacted with air, the particles underwent a strong exothermic oxidation reaction.

Batch Experiments. Amber bottles (125 mL, VWR) sealed with Mininert (VICI) caps and polytetrafluoroethylene (PTFE)/silicone septa (VWR) were used as anaerobic batch reactors for all compounds except DCA isomers. Bottles containing iron (generally 0.01−0.02 g) and water were prepared in the anaerobic chamber with minimal headspace (approximately 1 mL). Reactor and control bottles or vials (without iron) were prepared in duplicate. Reactions were initiated by injecting a known volume (typically 10−100 μL) of a methanolic stock solution of the chlorinated ethane; the resultant methanol volume fractions were less than 1%. Reactors and controls were mixed end-over-end at 40 rpm and room temperature (23 ± 1 °C). Due to short sampling intervals with HCA and PCA, multiple bottles were prepared with two sacrificed per sampling time. For tetra- and trichlorinated ethanes, duplicate bottles were prepared and sampled periodically by withdrawing 0.5 mL of the aqueous phase with a 1 mL airtight syringe (Hamilton), followed by injection of an equal volume of water or buffered water to maintain constant headspace. Aqueous samples were immediately injected into sealed 2 mL vials containing pentane (with 5 ppm toluene as an internal standard). After the bottles or vials were mixed thoroughly, 200 μL of the pentane extract was withdrawn and transferred to a gas chromatography (GC) autosampler vial. The transformations of the less reactive DCA isomers were monitored over 40 days in amber Environmental Protection Agency volatile organic analysis vials (24 mL, VWR) sealed with PTFE/silicone septa and open-top caps. Reactor preparation and sample handling was as described above except vials were sacrificed at each sampling time. Measurements of solution pH at initial and final times revealed increases from an initial pH of 7.2 to 7.8 (after 1−2 h), 7.9 (20 h), and 8.2 (120 h).

Analytical Methods. The analyses for chlorinated ethanes and chlorinated products were performed with a HP G1800A GCD gas chromatograph/mass spectrometer equipped with a DB-VRX column (60 m, 0.25 mm, 1.8 μm) (J&W Scientific). The temperature program was 70 °C for 8 min, 20 °C/min to 160 °C, and hold for 11 min. The sample (2 μL) was injected with a split ratio of 30:1. The carrier gas was ultra-high-purity (UHP) He at 1 mL/min, and the injector and detector temperatures were 230 and 300 °C, respectively. Selected ion monitoring (SIM) mode was used for data acquisition. No corrections were made for headspace partitioning of chlorinated compounds since this is expected to be less than 1% based on calculations for 1,1,1-TCA and 1,1-DCE (dimensionless Henry's Law constants 1.13 and 1.06, respectively) (*32*).

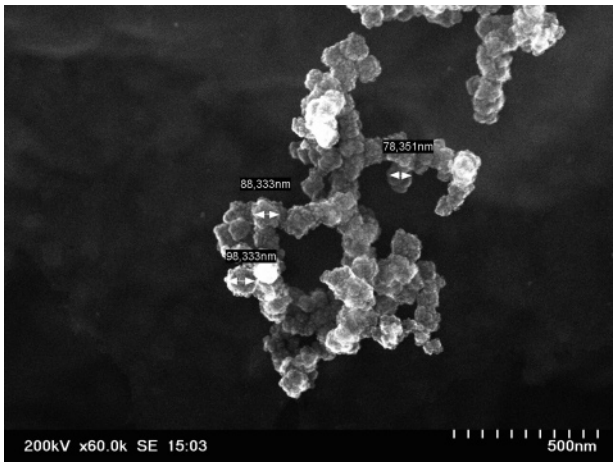

FIGURE 1. SEM image of nanosized iron.

For ethane and ethene analyses, 0.5 mL aqueous samples were removed from reactors and controls and placed in 2 mL crimp-cap GC vials. Vials were inverted, and the temperature was equilibrated at 25 °C for at least 8 h. Headspace samples (100 μL) were removed manually using a sample-lock syringe (Hamilton) and analyzed with a HP 5890 GC equipped with a GS-Q PLOT column (30 m, 0.545 mm, J&W Scientific) and flame ionization detector. The injection split ratio was 10:1, and the temperature was 230 °C. The oven temperature was 60 °C, and the UHP He carrier gas flow rate was 5.5 mL/min. The detector temperature was 300 °C. Aqueous concentrations of ethane and ethene were calculated using dimensionless Henry's Law constants at 25 °C as reported in the literature (20.4 for ethane and 8.75 for ethene) (*32*). The aqueous concentrations were further corrected for the fraction that partitioned into the 1 mL headspace.

Kinetic Modeling. Pseudo-first-order kinetic equations were used to fit the experimental data using the simplest possible pathways sufficient to describe the results. For compounds giving multiple products, parallel pathways converting parent compounds to initial products and, in some cases, pathways forming secondary products were postulated. Kinetic model equations in differential format are provided in the Supporting Information and described qualitatively in the Results and Discussion section. Experimental data for the parent compound removal and products generation were simultaneously fit by nonlinear least-squares methods using *Scientist for Windows* (version 2.01, Micromath). This software calculates 95% confidence intervals for each fitting parameter, and these are reported herein. Correlation coefficients and coefficients of determination were also calculated by the software, and these values are given in Supporting Information.

Results and Discussion

Characterization of Nanosized Iron. Figure 1 shows a scanning electron microscopy (SEM, Hitachi HD-2000) image of nanosized iron. As the image reveals, particles are uniform in size and shape with diameters in the range of 80−100 nm. The average specific surface area, measured by a Micromeritics ASAP 2010 using the Brunauer−Emmett−Teller Kr gas adsorption isotherm in the relative pressure range 0.06−0.21, was 27.9 ± 1.7 m^2/g for samples from five synthesis

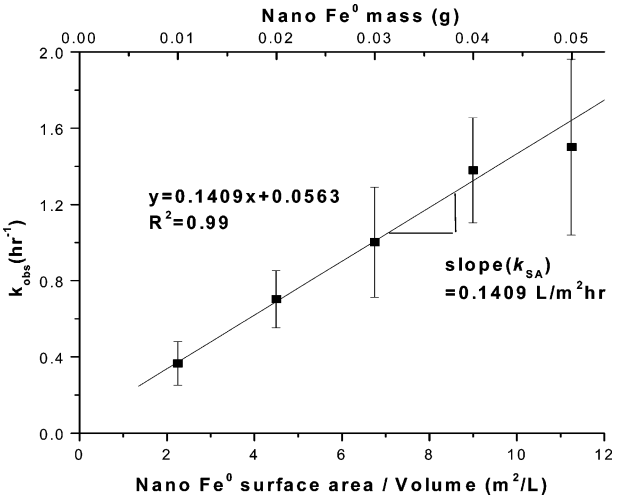

FIGURE 2. Correlation of the observed rate constant (k_{obs}) and metal loading (iron surface area concentration) in the reduction of 0.2 mM 1,1,1-TCA by nanosized iron in 124 mL of water. The slope of the line represents the surface-area-normalized rate constant (k_{SA}). Error bars represent 95% confidence limits.

batches. The particle composition measured by a Perkin-Elmer Sciex Elan 9000 inductively coupled plasma (ICP) mass spectrometer showed average iron and boron contents of 92 ± 0.4% and 7 ± 0.4%, respectively, for samples from six synthesis batches.

Effect of Metal Loading. The effect of metal loading on the reaction rate was studied using 0.2 mM 1,1,1-TCA and iron surface area concentrations ranging from 2.25 to 11.24 m^2/L as a check that linearity holds between the two variables. Figure 2 shows the plot of the pseudo-first-order rate constant for 1,1,1-TCA removal versus iron surface area concentration (iron mass). It shows that the rate constant increases linearly up to at least a loading of 0.04 g of iron per 124 mL. The slight flattening of the curve at the highest iron dose (0.05 g) is not statistically significant but could indicate a shift to mass-transfer-limited kinetics perhaps due to insufficient mixing. The surface normalized rate constant (k_{SA}) of 0.141 ± 0.007 L/m^2 h as determined by the slope of the regressed line is within experimental reproducibility of the value of 0.151 ± 0.013 L/m^2 h listed in Table 1, which was calculated by the simple normalization of the observed rate constant obtained from a single concentration versus the time data set. This result indicates that linearity between the reaction rate and the metal loading holds, at least over the range of iron loading tested.

Effect of Initial Concentration. The variability of observed rate constants with initial concentration can be used to test for adsorption-, surface-reaction-, or desorption-limited kinetics according to the Langmuir−Hinshelwood−Hougen−Watson (LHHW) model (*33*, *34*). Figure 3 shows the correlation between the observed rate constants and the initial concentration of PCA obtained from experiments in which 0.01 g of nanosized iron was reacted with 124 mL of 0.025−0.125 mM PCA. The results presented in the figure indicate relatively invariant pseudo-first-order rate constants for the initial concentration range investigated. The implication of this relationship may be that the reaction is not limited by the surface-reaction kinetics but by the adsorption of substrate before the reaction takes place. With commercial grade iron metals, deviation from pseudo-first-order kinetics has been observed to occur when surface reactive sites become saturated with substrates, leading to a decrease in reaction rate at high substrate concentrations and a transition to zero-order kinetics (*16*, *35*, *36*). In comparison to commercial grade iron metals, the nanosized iron prepared for this study is relatively free from nonreactive surface oxides. As a result, the reactivity of nanosized iron is likely to result in pseudo-first-order kinetics over a wider substrate concentration range. In view of additional reactivity results presented later in this paper, however, it is likely that the range of PCA concentration investigated is within the linear region of surface-reaction-limited kinetic behavior.

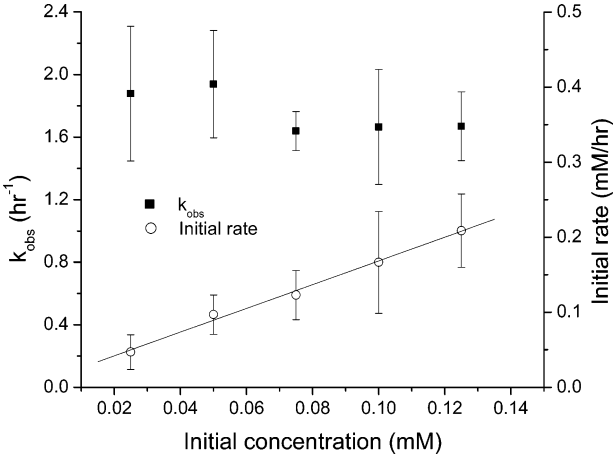

FIGURE 3. Effect of the initial concentration of the target compound on the pseudo-first-order rate constant (k_{obs}) and the initial rate ($k_{obs}C_0$) in the reduction of PCA by 0.01 g of nanosized iron per 124 mL of water. Error bars represent 95% confidence limits.

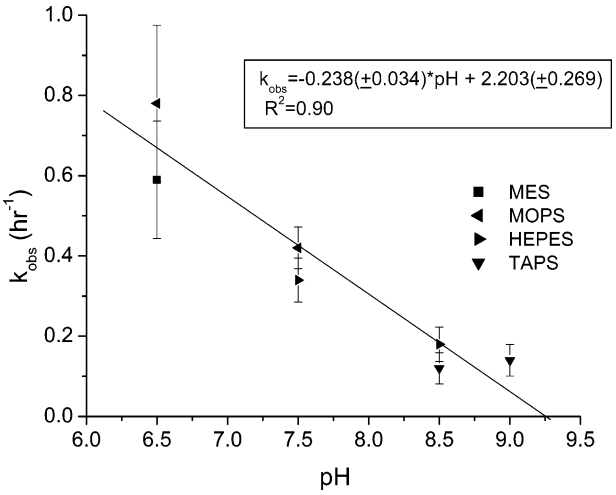

FIGURE 4. Effect of pH on the pseudo-first-order rate constant for 1,1,2,2-TeCA reduced by nanosized iron. Error bars represent 95% confidence limits.

Effect of pH. Neutral and base hydrolysis are known to be important reactions for several chlorinated ethanes. Results of the study by Jeffers et al. (*8*) indicate that the rate constants for hydrolysis or dehydrohalogenation at pH 7 and above are most significant for PCA and 1,1,2,2-TeCA. The rate constants for other chlorinated ethanes except 1,1,1-TCA are smaller by 2 orders of magnitude or more. Similarly, pH is known to affect rates of reactions with zero-valent iron due to effects on iron corrosion, producing more corrosion at lower pH values and more passivation by mineral precipitation at higher pH values (*37*, *38*). To investigate the interplay of these effects, the reduction of 1,1,2,2-TeCA was examined using a series of organic buffers. Solutions of pH 6.5−9 were prepared by using four different buffers at 50 mM total concentration. Each target pH, except pH 9, was obtained using two buffers to check for possible buffer effects. The reactions were carried out with 0.05 g of nanosized iron and 124 mL of 50 mM 1,1,2,2-TeCA.

TABLE 1. Reaction Products, Reaction Pathways, Observed Pseudo-First-Order Rate Constants (k_{obs}) and Surface-Area-Normalized Rate Constants (k_{SA}) for the Reduction of Chlorinated Ethanes[a]

reactant	reaction pH range	initial products	reaction pathway	k_{obs}[b] (h^{-1})	Σk_{obs}[c] (h^{-1})	Σk_{SA}[c,d] (L m^{-2} h^{-1})	literature k_{SA} (L m^{-2} h^{-1})
HCA	7.2−7.8	PCE	β-elimination	$1.73 (\pm 0.12) \times 10^{0}$	$1.73 (\pm 0.12) \times 10^{0}$	$7.70 (\pm 0.70) \times 10^{-1}$	3.1×10^{-2} [e] 7.4×10^{-2} [f]
PCA	7.2−7.8	PCE TCE	dehydrohalogenation β-elimination	$2.06 (\pm 0.48) \times 10^{-1}$ $1.59 (\pm 0.08) \times 10^{0}$	$1.79 (\pm 0.09) \times 10^{0}$	$7.96 (\pm 0.63) \times 10^{-1}$	
1,1,1,2-TeCA	7.2−7.9	TCE 1,1-DCE	dehydrohalogenation β-elimination	$5.7 (\pm 7.7) \times 10^{-2}$ $1.15 (\pm 0.07) \times 10^{0}$	$1.21 (\pm 0.10) \times 10^{0}$	$5.38 (\pm 0.56) \times 10^{-1}$	1.4×10^{-2} [e] 2.1×10^{-3} [f]
1,1,2,2-TeCA	7.2−8.2	TCE *trans*-DCE *cis*-DCE	dehydrohalogenation β-elimination β-elimination	$1.84 (\pm 0.42) \times 10^{-2}$ $1.72 (\pm 0.52) \times 10^{-2}$ $3.26 (\pm 0.53) \times 10^{-2}$	$6.82 (\pm 0.85) \times 10^{-2}$	$3.03 (\pm 0.42) \times 10^{-2}$	1.3×10^{-2} [e] 5.0×10^{-4} [f]
1,1,1-TCA	7.2−8.0	1,1-DCA ethane	hydrogenolysis α-elimination + hydrogenolysis	$2.44 (\pm 0.15) \times 10^{-1}$ $9.7 (\pm 1.3) \times 10^{-2}$	$3.40 (\pm 0.20) \times 10^{-1}$	$1.51 (\pm 0.13) \times 10^{-1}$	1.1×10^{-2} [e] 1.8×10^{-3} [f] 4.6×10^{-1} [g]
1,1,2-TCA	7.2−8.2	ethane	β-elimination + hydrogenolysis	$5.20 (\pm 0.71) \times 10^{-3}$	$5.20 (\pm 0.71) \times 10^{-3}$	$2.31 (\pm 0.34) \times 10^{-3}$	
1,1-DCA	7.2−8.6	ethane	α-elimination	$2.41 (\pm 0.52) \times 10^{-4}$	$2.41 (\pm 0.52) \times 10^{-4}$	$1.99 (\pm 0.44) \times 10^{-5}$	
1,2-DCA	7.2−8.6			$< 5 \times 10^{-5}$ [h]	$< 5 \times 10^{-5}$	$< 4 \times 10^{-6}$	

[a] Reaction conditions: 23 ± 1 °C, 0.01 g of nanosized iron in 124 mL of solution except 1,1- and 1,2-DCA which were reacted in 24 mL of solution. [b] Uncertainties represent 95% confidence limits. [c] Reported 95% confidence limits determined by error propagation calculations. [d] k_{SA} values were calculated using an iron surface area of 27.9 (±1.7) m^2/g. [e] Johnson et al. (*16*), results from an analysis of literature kinetic data. [f] Gillham and O'Hannesin (*15*), 100 mesh Fisher electrolytic iron, surface area 0.287 m^2/g, reaction at room temperature. [g] Fennelly and Roberts (*13*), 100 mesh Fisher electrolytic iron, surface area 0.16 m^2/g, reaction at room temperature. [h] Upper limit estimation based on less than 5% conversion over 40 days.

The pseudo-first-order rate constants obtained are plotted against pH in Figure 4. The result shows a general trend of decreasing reaction rate with increasing pH, consistent with the result observed for $CHCl_3$ and TCE reduction (*22*, *25*) and other previously reported studies conducted under similar conditions (*37*, *38*). Linear regression of the data results in a reasonable correlation coefficient between pH and the rate constants despite some scatter attributable to buffer effects. The slope (0.24 h^{-1}/pH) is much smaller than the slope of 1.08 h^{-1}/pH (and reaction order 0.15) obtained by Matheson and Tratnyek for CCl_4 with microsized iron. This indicates that the nanosized iron synthesized in this work is more reactive and less passivated by crystalline iron minerals than commercial irons, consistent with results recently reported by Liu et al. (*23*). The observed slope is smaller than that obtained using $CHCl_3$ and TCE (0.33 and 0.90 h^{-1}/pH, respectively) (*22*, *25*), reflecting the increasing contribution of dehydrohalogenation with increasing pH.

Direct evidence of increased dehydrohalogenation can be found by examining the product distribution ratio. The concentration ratio of TCE to DCE isomers at the last sampling time is 1.3 at pH 9 with TAPS buffer, which can be translated into approximately 57% of overall removal via dehydrohalogenation. In comparison to approximately 27% dehydrohalgenation at pH 7.5, a 2-fold increase of dehydrohalogenation occurred. In addition, the observed pseudo-first-order rate constant at pH 9 is about 0.02 h^{-1} greater than at pH 8.5. Although not statistically significant, this is likely an indication that the rate of dehydrohalogenation has exceeded the rate of β-elimination.

Taken together, these results indicate that below approximately pH 7.5 the observed rate constant for 1,1,2,2-TeCA reflects minor contributions from dehydrohalogenation, whereas at pH values above 8 it is significant. Analysis of products and kinetic modeling can be used to separately quantify the two processes. In comparison to 1,1,2,2-TeCA, β-elimination of PCA is nearly 2 orders of magnitude more rapid (see next section), and dehydrohalogenation is about 1 order of magnitude more rapid. Therefore, the influence of increasing pH and dehydrohalogenation on PCA will be less than that observed for 1,1,2,2-TeCA. Similarly, β-elimination is rapid for 1,1,1,2-TeCA, and dehydrohalogenation is not significant. For the tri- and dichlorinated ethanes, both electron transfer and dehydrohalogenation rates are slower. The relative contributions are difficult to measure because the dehydrohalogenation products (DCEs and VC) react rapidly with Fe^0 (22). In general, the low reaction order of H^+ indicates relatively small indirect effects on the electron-transfer kinetics.

Reduction of Chlorinated Ethanes. Chlorinated ethanes showed a wide spectrum of reactivity from virtually nondegradable to almost instantaneously transformable when reacted with nanosized iron. The reaction products resulting from different pathways, pseudo-first-order rate constants (k_{obs}), and surface-area-normalized rate constants (k_{SA}) obtained from reduction of eight chlorinated ethanes are given in Table 1. Note that for compounds giving multiple products rate constants corresponding to the formation of each initial product were calculated assuming parallel pathways. The overall rate constants were then obtained by summing the individual rate constants. For comparison, k_{SA} values reported in the literature using commercial grade microsized iron as a reductant are also included in Table 1. While better indicators of iron reactivity are being pursued (*39*), the k_{SA} parameter is the only possible basis for comparison at this time and with available results.

The rate constants presented in Table 1 were obtained from simultaneously fitting data for parent compound removal and product generation. Except for 1,1,2-TCA and 1,1-DCA, pseudo-first-order fits to parent compound disappearance alone give rate constants that are approximately 10−20% higher than the Σk_{obs} results presented and overestimate the parent compound initial concentrations by up to 16%. These initial concentrations are well supported by control measurements, and the simultaneous fitting procedure uniformly predicts initial concentrations in excellent agreement with controls. Small deviations from first-order behavior may be due to changes in the iron surface as the dry particles are exposed to aqueous solution in the initial phases of the reactions. Simultaneous fitting gives the best overall description of the total experimental data.

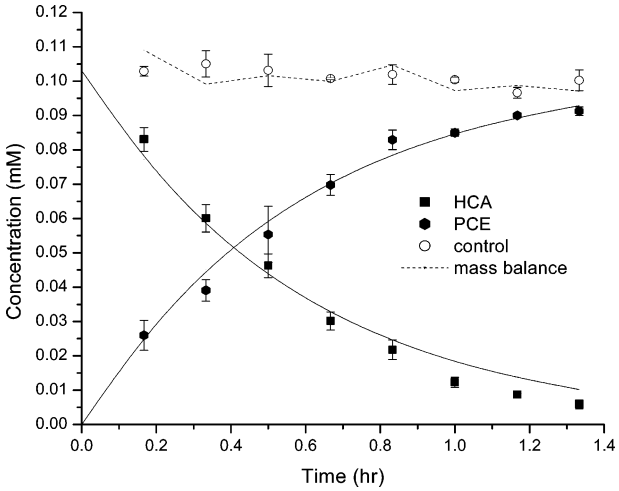

FIGURE 5. Reduction of HCA by 0.01 g of nanosized iron in 124 mL of water. Smooth lines represent the pseudo-first-order fitting of the data points. Symbols are the average concentrations from duplicate reactors or controls, and error bars represent the range of concentrations. In some cases, error bars are smaller than the symbol.

It is generally accepted that the rate-limiting step in the reduction of chlorinated aliphatic compounds is the transfer of a single electron and the formation of an alkyl radical (*14*). The reactivity of chlorinated ethanes reported herein is consistent with this in that the reaction rate tends to increase with increasing chlorination and also depends on the positions of the chlorines. Such a dependence suggests the importance of the reduction potential of the molecule. Results for individual compounds and isomer groups are presented in turn below, followed by a structure−reactivity relationship analysis.

HCA. HCA was one of the most reactive compounds studied. As shown in Figure 5, reaction with nanosized iron gave rise to PCE as the major reaction product, consistent with previously reported studies using zero-valent zinc (*10*) and iron sulfide (*40*). Disappearance of HCA and formation of PCE were well fitted by pseudo-first-order kinetics with good mass balance throughout the reaction period (95%) and good agreement between the molar balance of C_2-hydrocarbons and the controls.

Only two studies to date report HCA reduction by iron metal (*15*, *16*), but no information on reaction products was provided. However, the similarity between reaction products observed in this study and in studies using zinc (*10*) and FeS (*40*) suggests a common reaction pathway. In each study, the main product was PCE formed via reductive β-elimination, in which two chlorine atoms from adjacent carbons are removed, followed by the formation of a double bond. Trace amounts of PCA were detected in this study and by Butler and Hayes (*40*) and are thought to result from hydrogenolysis (replacement of chlorine with hydrogen). The transformation of HCA by reductive β-elimination or hydrogenolysis involves the formation of a pentachloroethyl radical as an initial step, followed by acceptance of an electron to form the pen-

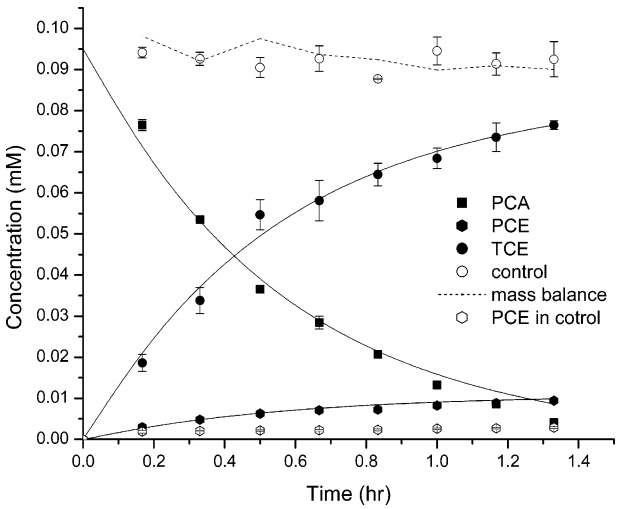

FIGURE 6. Reduction of PCA by 0.01 g of nanosized iron in 124 mL of water. Smooth lines represent the pseudo-first-order fitting of the data points. Symbols are the average concentrations from duplicate reactors or controls, and error bars represent the range of concentrations. In some cases, error bars are smaller than the symbol.

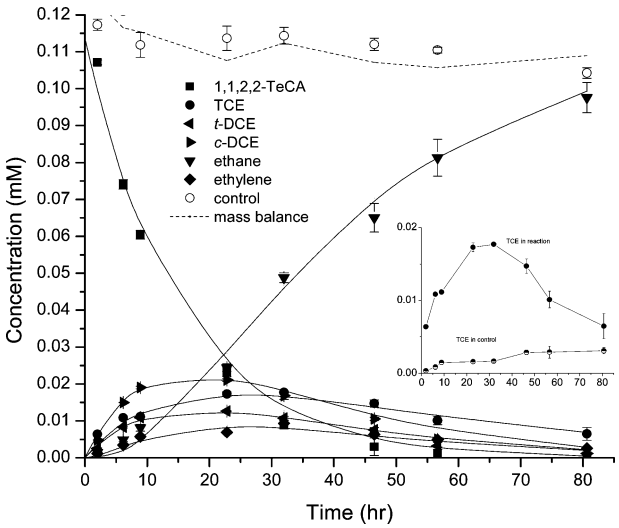

FIGURE 7. Reduction of 1,1,2,2-TeCA by 0.01 g of nanosized iron in 124 mL of water. The figure inset shows TCE concentrations in reactor and control bottles. Smooth lines represent the pseudo-first-order fitting of the data points. Symbols are the average concentrations from duplicate reactors or controls, and error bars represent the range of concentrations. In some cases, error bars are smaller than the symbol.

tachloroethyl anion. This carbanion species then either loses chloride in an antiplanar position, followed by double bond formation, to form PCE (β-elimination) or accepts a proton to form PCA (hydrogenolysis). PCA may also be formed through hydrogen abstraction by the pentachloroethyl radical. The predominance of β-elimination over hydrogenolysis may be partially due to the rapidity of intermolecular rearrangements compared to bimolecular collisions with H^+ at moderately basic pHs or with abstractable hydrogens. Also, the possibility of direct formation of PCE from the pentachloroethyl radical by transfer of a second electron and concurrent carbon−chlorine bond breaking cannot be ruled out since evidence for such a concerted pathway has been reported in the dihaloelimination of vicinal dibromoalkanes (*41*).

PCA. PCA was transformed to PCE and TCE as shown in Figure 6. The product branching ratio, defined as the ratio of rate constants for two parallel reactions ($k_{PCA\rightarrow TCE}/k_{PCA\rightarrow PCE}$) (*42*) was 7.7 ± 2.9. The formation of PCE is of interest, for this transformation can occur without electron transfer. Direct nucleophilic substitution by a Brønsted base such as OH^- is sterically hindered, but the somewhat acidic β-hydrogen may be attacked. The resulting carbanion may eliminate chloride from an antiplanar position and form a double bond (*43*). Although PCE and TCE are also subject to reduction by iron, the rates are slower, (*22*) and their conversions over the time scale of PCA reduction are insignificant.

Arnold et al. (*10*) observed similar reaction products in PCA reduction by zinc metal at a constant pH of 7.5. In their study, PCE formation accounted for approximately 7% ($k \approx$ 0.05 h^{-1}) of overall PCA transformation, and essentially identical PCE formation in reactions and controls suggested that dehydrohalogenation was unaffected by the presence of zinc. As shown graphically in the Supporting Information (Figure S1), the dehydrohalogenation rate constant obtained in this study in controls at pH 7.2 ± 0.3 is in excellent agreement with three other studies (*8*−*10*). The predicted homogeneous dehydrohalogenation rate constant at the final pH of the iron-containing reactors (*7*, *8*) can account for approximately 40% of PCA removal by dehydrohalogenation in those reactors, indicating significant surface-promoted dehydrohalogenation. Similar surface-promoted dehydrohalogenation of PCA has been observed for reaction between commercial iron and PCA and may be attributable to increases in pH and surface sites containing ferrous iron (*44*).

TeCA Isomers. Figure 7 shows the timecourse for the reduction of 1,1,2,2-TeCA. Similar data for the reduction of 1,1,1,2-TeCA are shown in Figure S2 (Supporting Information). The k_{SA} values for two TeCA isomers obtained in this study are 1−2 orders of magnitude greater than the values reported in the literature for commercial grade microsized iron metal (Table 1). Also note that the k_{SA} calculated for 1,1,2,2-TeCA loss at pH 8 shown in Figure 4, 2.7×10^{-2} L m^{-2} h^{-1} (0.05 g of Fe/124 mL), agrees well with the result shown in Table 1. As previously mentioned, there is a substantial difference in the reaction rate between the two isomers. Reductive β-elimination was the major pathway for 1,1,1,2-TeCA transformation to produce 1,1-DCE, accounting for approximately 95% of the total 1,1,1,2-TeCA disappearance, while dehydrohalogenation to TCE accounted for 5%. The ethane and ethene observed are the secondary reaction products from subsequent reduction of 1,1-DCE and TCE (*22*).

The reduction of 1,1,2,2-TeCA proceeded with a somewhat different ratio of the two concurrent initial pathways such that β-elimination to form two DCE isomers (*cis*- and *trans*-DCE) and dehydrohalogenation to form TCE accounted for approximately 73% and 27%, respectively. Ethane and ethene are again observed as secondary reduction products. The greater removal of 1,1,2,2-TeCA by dehydrohalogenation compared to that of 1,1,1,2-TeCA is primarily due to slower removal by β-elimination (due to lack of a carbon with trisubstitution by chlorine). More rapid hydrolysis of 1,1,2,2-TeCA than 1,1,1,2-TeCA was observed by Jeffers et al. (*8*), with a rate constant approximately 2 orders of magnitude greater at pH 7. From control reactors, we determined a dehydrohalogenation rate constant for 1,1,2,2-TeCA at pH 7.2 that is approximately 5.5 times greater than would be predicted by Jeffers et al. (*8*). However, results of a measurement at pH 9 by Haag and Mill (*7*) are 5.8 times greater than the Jeffers et al. prediction (*8*). TCE concentrations from reaction and control reactors are compared in the inset of Figure 3. As observed for PCA, the extent of dehydrohalogenation in the presence of iron (0.018 h^{-1}) was greater than

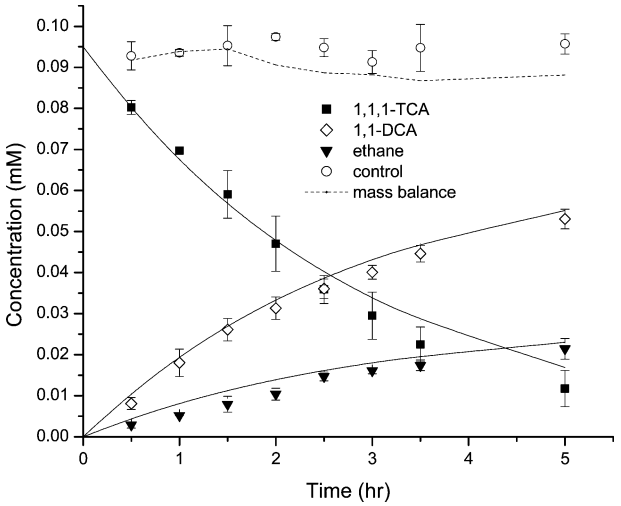

FIGURE 8. Reduction of 1,1,1-TCA by 0.01 g of nanosized iron in 124 mL of water. Smooth lines represent the pseudo-first-order fitting of the data points. Symbols are the average concentrations from duplicate reactors or controls, and error bars represent the range of concentrations. In some cases, error bars are smaller than the symbol.

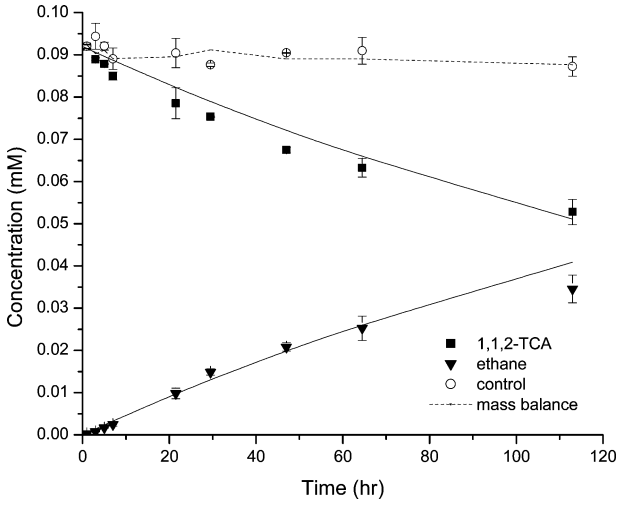

FIGURE 9. Reduction of 1,1,2-TCA by 0.01 g of nanosized iron in 124 mL of water. Lines represent the pseudo-first-order fitting of the data points

that in controls (0.0016 h^{-1}), presumably due to higher pH and surface-mediated processes.

The product branching ratio for *cis*-DCE and *trans*-DCE in the reduction of 1,1,2,2-TeCA was 1.89 ± 0.65 (Table 1), indicating the formation of *cis*-DCE was favored. Arnold et al. (*17*) used a simplified Marcus theory approach and predicted a ratio of 1.84−1.96 for iron metal as the reductant. The product ratio obtained from this study is in good agreement with that prediction whereas the experimental product ratio obtained by Arnold et al. (*17*) was much higher (4.5). They attributed the disparity to the formation of a surface organometallic complex that controlled product distribution. Our results may serve to advance this interpretation by contrasting reactions on iron surfaces of different characteristics and histories. The surfaces of the nanosized iron used in our study should be relatively free of crystalline iron oxides. Commercially available iron is typically exposed to air during use and storage, leading to the formation of oxides such as hematite (*45*, *46*) that may be incompletely removed even with acid pretreatment. Thus, we suggest that the product ratio observed by Arnold et al. was controlled by a surface complex with crystalline oxides, whereas our ratio reflects interactions of reaction intermediates with an iron surface covered with amorphous iron (hydr)oxides. Liu et al. (*23*) observed higher reactivity for TCE reduction and an absence of particle surface deactivation with nanosized iron particles compared to nanoparticles with a crystalline, insoluble Fe_3O_4 shell. They proposed the more reactive amorphous materials may permit closer access to Fe^0 and/or better transfer of electrons.

TCA Isomers. Reduction of 1,1,1-TCA and 1,1,2-TCA are shown in Figures 8 and 9, respectively. 1,1,1-TCA reacted relatively rapidly to yield 1,1-DCA and ethane as the major products. The hydrogenolysis pathway, generating 1,1-DCA, accounted for approximately 69% of the overall 1,1,1-TCA disappearance. The formation of ethane, however, cannot be explained by a single pathway. Further, as Figure 8 reveals, ethane appears to evolve almost simultaneously with 1,1-DCA, too early to be attributable to the production and subsequent reduction of 1,1-DCA. Therefore, a concerted reaction pathway involving α-elimination and hydrogenolysis is likely. Concerted pathways have been proposed by Fennelly and Roberts (*13*) for the formation of ethane from 1,1,1-TCA reduction by microsized iron. These are similar to the pathways proposed for methane formation from CCl_4 by McCormick and Adriaens (*47*) and from CCl_4 or $CHCl_3$ (*26*) in that it involves sequential electron transfer to the carbon, spontaneous ejection of chloride, and proton attachment to the lone pairs of electrons on the carbon. A detailed mechanistic pathway depicting ethane formation from 1,1,1-TCA is included in the Supporting Information.

Reduction of 1,1,2-TCA proceeded at a much slower rate (Figure 9). Because of the chlorine atoms in the α- and β-positions, it can undergo β-elimination. Reductive β-elimination of 1,1,2-TCA would have given vinyl chloride as a product, as observed in a previously reported study with zinc metal (*10*). Ethane was the sole observed product and vinyl chloride was not detected in this study. It is likely that vinyl chloride was produced but maintained at concentrations below detection limits (0.062 ppm) by rapid reaction with nanosized zero-valent iron to form ethane ($k_{SA} \approx 0.6$ L m^{-2} h^{-1} (*22*)).

DCA Isomers. 1,1-DCA reacted with iron at a much slower rate than species bearing more chlorine atoms (Figure S3). Ethane was the sole reaction product and is assumed to have evolved via α-elimination. This slow rate of reduction is consistent with the hypothesis of a direct pathway from 1,1,1-TCA to ethane. Fennelly and Roberts (*13*) also demonstrated that 1,1-DCA reacts too slowly to be an intermediate in the formation of ethane or ethene from the reduction of 1,1,1-TCA.

1,2-DCA showed no appreciable sign of transformation over 40 days of reaction. Although evidence of β-elimination of 1,2-DCA to form ethane was reported with zero-valent zinc (*10*), analyses performed in this study did not give any evidence of ethane formation.

Quantitative Structure−Reactivity Relationships. As suggested by Arnold and Roberts (*48*) and Scherer et al. (*49*), the fact that the reduction of chlorinated ethanes is likely to proceed through direct electron transfer with the transfer of the first electron to form alkyl radical species as the rate-limiting step suggests that parameters such as one-electron reduction potentials (E1) and lowest unoccupied molecular orbital (LUMO) energies may be predictive of their reactivity with nanosized iron. Figure 10 shows linear free energy relationships for log k_{SA} versus E1 and versus LUMO energies. LUMO and E1 values for chlorinated ethanes were obtained from the literature (*49*, *50*). Note that when there are multiple possible radical species that can be formed from a given compound (e.g., PCA, 1,1,1,2-TeCA, and 1,1,2-TCA) the E1 value for the more thermodynamically favorable species was

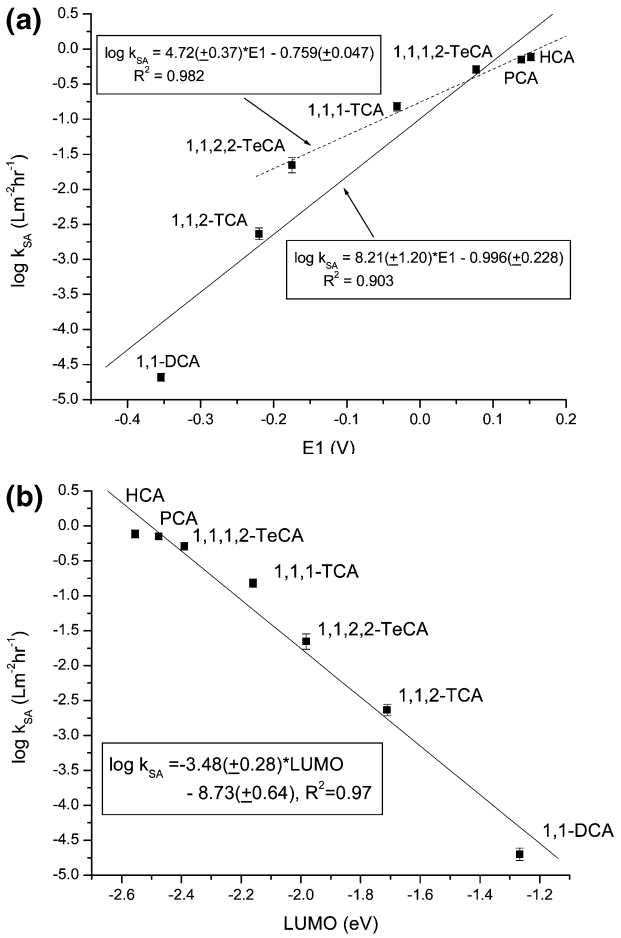

FIGURE 10. Correlation of the surface-area-normalized rate constant (k_{SA}) with (a) the one-electron reduction potential (E1) and (b) the lowest unoccupied molecular orbital (LUMO) energy of chlorinated ethanes. The contribution of dehydrohalogenation was excluded in the calculation of k_{SA} values shown. Regression equations show standard errors for slopes and intercepts.

used. Also, if dehydrohalogenation was one of multiple pathways observed in removal of the compound, then its contribution was excluded in the overall k_{SA} values shown in the figure, since dehydrohalogenation does not involve electron transfer.

A reasonable linear correlation of log k_{SA} with E1 (R^2 = 0.90) was found, suggesting the formation of radical species is important in controlling the rates of reduction of chlorinated ethanes. From methods described by Arnold et al. (*10*), calculations showed that mass transfer limitations are not significant for HCA and PCA. The ratio $k_L a/k_{obs}$, where $k_L a$ is the product of the mass transfer coefficient (k_L, ms^{-1}) and the ratio of the geometric metal surface area to solution volume (a, m^{-1}) and k_{obs} is the observed rate constant (s^{-1}), is an indication of the relative magnitudes of mass transfer and observed reaction rates. The estimated value of 10^5 for 50 nm diameter particles shows mass transfer is expected to be very rapid compared to reaction and will not influence k_{obs} values. Even if agglomeration were to produce particles 1000 nm in diameter, the ratio is approximately 10^2. If the two least reactive compounds, 1,1-DCA and 1,1,2-TCA, are neglected, then the R^2 value increases to 0.98, as shown in Figure 10. Less effective adsorption of these compounds may contribute to low k_{obs} values; however, correlations with parameters such as solubility and K_{ow} were poor.

In contrast, the correlation with LUMO values is much better across the range of seven compounds (R^2 = 0.97). However, our experimental data indicate the loss of 1,2-DCA is very slow with a k_{SA} of less than 4×10^{-6} (L m^{-2} h^{-1}) The correlation using E1 would predict a low reaction rate constant for 1,2-DCA (E1 = −0.558 V (*50*), $k_{SA} = 2.6 \times 10^{-6}$ L m^{-2} h^{-1}) whereas the LUMO correlation predicts approximately equal reactivity for both 1,1- and 1,2-DCA (LUMO = −1.183 eV (*49*), $k_{SA} = 2.4 \times 10^{-5}$ L m^{-2} h^{-1}).

Both parameters are strong but incomplete predictors of the reaction rate constants for the group of eight chlorinated ethanes. Because of the interplay of different processes (e.g., adsorption, electron transfer from an iron surface, surface passivation), a single parameter may not control reaction rates across the range of chlorinated ethane properties. Incomplete or improper accounting for the contribution of dehydrohalogenation to k_{SA} may also contribute to nonlinearities in these correlations. Despite these limitations and uncertainties, the LFERs developed here support the dominance of electron transfer in predicting reaction rates with the iron synthesized in this work. These relationships should hold potential for predicting the reactivity of other chlorinated aliphatic species with nanosized iron.

Acknowledgments

This work was supported by the National Science Foundation (Award No. 996394) and the South Carolina Commission on Higher Education (Award No. R00-C05).

Supporting Information Available

Complete kinetic model equations in differential equation format, goodness-of-fit parameters for kinetic modeling results, linear correlation of homogeneous PCA dehydrohalogenation rate constants with pH among four independent studies, the reduction of 1,1,1,2-TeCA, the reduction of 1,1-DCA, and a proposed mechanistic pathway for 1,1,1-TCA transformation by nanosized iron. This material is available free of charge via the Internet at http://pubs.acs.org.

Literature Cited

(1) U.S. Environmental Protection Agency. *Common Chemicals Found at Superfund Sites*; EPA 540/R-94/044; Office of Emergency and Remedial Response: Washington, DC, 1994.

(2) U.S. Environmental Protection Agency. *Edition of the Drinking Water Standards and Health Advisories*; EPA 822/R-04/005; Office of Water: Washington, DC, 2004.

(3) Vogel, T. M.; Criddle, C. S.; McCarty, P. L. Transformations of halogenated aliphatic compounds. *Environ. Sci. Technol.* **1987**, *21*, 722−736.

(4) Chen, C.; Puhakka, J. A.; Ferguson, J. F. Transformations of 1,1,2,2-tetrachloroethane under methanogenic conditions. *Environ. Sci. Technol.* **1996**, *30*, 542−547.

(5) Schanke, C. A.; Wackett, L. P. Environmental reductive elimination reactions of polychlorinated ethanes mimicked by transition-metal coenzymes. *Environ. Sci. Technol.* **1992**, *26*, 830−833.

(6) Thompson, J. A.; Ho, B.; Mastovich, S. L. Dynamic headspace analysis of volatile metabolites from the reductive dehalogenation of trichloroethanes and tetrachloroethanes by hepatic microsomes. *Anal. Biochem.* **1985**, *145*, 376−384.

(7) Haag, W. R.; Mill, T. Effect of a subsurface sediment on hydrolysis of haloalkanes and epoxides. *Environ. Sci. Technol.* **1988**, *22*, 658−663.

(8) Jeffers, P. M.; Ward, L. M.; Woytowitch, L. M.; Wolfe, N. L. Homogeneous hydrolysis rate constants for selected chlorinated methanes, ethanes, ethenes, and propanes. *Environ. Sci. Technol.* **1989**, *23*, 965−969.

(9) Roberts, A. L.; Gschwend, P. M. Mechanism of pentachloroethane dehydrochlorination to tetrachloroethylene. *Environ. Sci. Technol.* **1991**, *25*, 76−86.

(10) Arnold, W. A.; Ball, W. P.; Roberts, A. L. Polychlorinated ethane reaction with zero-valent zinc: Pathways and rate control. *J. Contam. Hydrol.* **1999**, *40*, 183−200.

(11) Butler, E. C.; Hayes, K. F. Kinetics of the transformation of halogenated aliphatic compounds by iron sulfide. *Environ. Sci. Technol.* **2000**, *34*, 422−429.

(12) Klecka, G. M.; Carpenter, C. L.; Gonsior, S. J. Biological transformations of 1,2-dichloroethane in subsurface soils and groundwater. *J. Contam. Hydrol.* **1998**, *34*, 139−154.
(13) Fennelly, J. P.; Roberts, A. L. Reaction of 1,1,1-trichloroethane with zero-valent metals and bimetallic reductants. *Environ. Sci. Technol.* **1998**, *32*, 1980−1988.
(14) Vogel, T. M.; McCarty, P. L. Abiotic and biotic transformations of 1,1,1-trichloroethane under methanogenic conditions. *Environ. Sci. Technol.* **1987**, *21*, 1208−1213.
(15) Gillham, R. W.; O'Hannesin, S. F. Enhanced degradation of halogenated aliphatics by zero-valent iron. *Ground Water* **1994**, *32*, 958−967.
(16) Johnson, T. L.; Scherer, M. M.; Tratnyek, P. G. Kinetics of halogenated organic compound degradation by iron metal. *Environ. Sci. Technol.* **1996**, *30*, 2634−2640.
(17) Arnold, W. A.; Winget, P.; Cramer, C. J. Reductive dechlorination of 1,1,2,2-tetrachloroethane. *Environ. Sci. Technol.* **2002**, *36*, 3536−3541.
(18) Schreier, C. G.; Reinhard, M. Transformation of chlorinated organic compounds by iron and manganese powders in buffered water and in landfill leachate. *Chemosphere* **1994**, *29*, 1743−1753.
(19) Zhang, W. X.; Wang, C. B.; Lien, H. L. Treatment of chlorinated organic contaminants with nanoscale bimetallic particles. *Catal. Today* **1998**, *40*, 387−395.
(20) Lien, H. L.; Zhang, W. X. Nanoscale iron particles for complete reduction of chlorinated ethenes. *Colloids Surf., A* **2001**, *191*, 97−105.
(21) Schrick, B.; Blough, J. L.; Jones, A. D.; Mallouk, T. E. Hydrodechlorination of trichloroethylene to hydrocarbons using bimetallic nickel−iron nanosized particles. *Chem. Mater.* **2002**, *14*, 5140−5147.
(22) Song, H.; Carraway, E. R. Reduction of chlorinated ethenes by nanosized zero-valent iron., to be submitted for publication.
(23) Liu, Y.; Majetich, S. A.; Tilton, R. D.; Sholl, D. S.; Lowry, G. V. TCE dechlorination rates, pathways, and efficiency of nanoscale iron particles with different properties. *Environ. Sci. Technol.* **2005**, *39*, 1338−1345.
(24) Lien, H. L.; Zhang, W. X. Transformation of chlorinated methanes by nanoscale iron particles. *J. Environ. Eng.* **1999**, *125*, 1042−1047.
(25) Choe, S.; Lee, S. H.; Chang, Y. Y.; Hwang, K. Y.; Khim, J. Rapid reductive destruction of hazardous organic compounds by nanoscale Fe-0. *Chemosphere* **2001**, *42*, 367−372.
(26) Song, H.; Carraway, E. R. Reduction of chlorinated methanes by nanosized zero-valent iron. *Environ. Eng. Sci.*, submitted for publication.
(27) Xu, Y.; Zhang, W. X. Subcolloidal Fe/Ag particles for reductive dehalogenation of chlorinated benzenes. *Ind. Eng. Chem. Res.* **2000**, *39*, 2238−2244.
(28) Ponder, S. M.; Darab, J. G.; Bucher, J.; Caulder, D.; Craig, I.; Davis, L.; Edelstein, N.; Lukens, W.; Nitsche, H.; Rao, L. F.; Shuh, D. K.; Mallouk, T. E. Surface chemistry and electrochemistry of supported zerovalent iron nanoparticles in the remediation of aqueous metal contaminants. *Chem. Mater.* **2001**, *13*, 479−486.
(29) Ponder, S. M.; Darab, J. G.; Mallouk, T. E. Remediation of Cr(VI) and Pb(II) aqueous solutions using supported, nanoscale zero-valent iron. *Environ. Sci. Technol.* **2000**, *34*, 2564−2569.
(30) Choe, S.; Chang, Y. Y.; Hwang, K. Y.; Khim, J. Kinetics of reductive denitrification by nanoscale zerovalent iron. *Chemosphere* **2000**, *41*, 1307−1311.
(31) Glavee, G. N.; Klabunde, K. J.; Sorensen, C. M.; Hadjipanayis, G. C. Chemistry of borohydride reduction of iron(II) and iron-(III) ions in aqueous and nonaqueous media−formation of nanoscale Fe, FeB, and Fe_2B powders. *Inorg. Chem.* **1995**, *34*, 28−35.
(32) Mackay, D.; Shiu, W. Y. A Critical review of Henry's Law constants for chemicals of environmental interest. *Environ. Sci. Technol.* **1981**, *10*, 1175−1199.
(33) Fogler, S. *Elements of Chemical Reaction Engineering*, 2nd ed.; Prentice Hall: Englewood Cliffs, NJ, 1992.
(34) Arnold, W. A. Kinetics and pathways of chlorinated ethylene and chlorinated ethane reaction with zero-valent metals. Ph.D. Dissertation, The Johns Hopkins University, Baltimore, MD, 1999.
(35) Zepp, R. G.; Wolfe, N. L. Abiotic transformation of organic chemicals at the particle−water interface; In *Aquatic Surface Chemistry: Chemical Processes at the Particle−Water Interface*; Stumm, W., Ed.; Wiley: New York, 1987.
(36) Wust, W. F.; Kober, R.; Schlicker, O.; Dahmke, A. Combined zero- and first-order kinetic model of the degradation of TCE and *cis*-DCE with commercial iron. *Environ. Sci. Technol.* **1999**, *33*, 4304−4309.
(37) Matheson, L. J.; Tratnyek, P. G. Reductive dehalogenation of chlorinated methanes by iron metal. *Environ. Sci. Technol.* **1994**, *28*, 2045−2053.
(38) Alowitz, M. J.; Scherer, M. M. Kinetics of nitrate, nitrite, and Cr(VI) reduction by iron metal. *Environ. Sci. Technol.* **2002**, *36*, 299−306.
(39) Cwiertny, D. M.; Roberts, A. L. Nonlinear influence of iron mass loading on the reduction of chlorinated solvents. *Prepr. Ext. Abstr. ACS Natl. Meet., Am. Chem. Soc., Div. Environ. Chem.* **2004**, *44*, 923−928.
(40) Butler, E. C.; Hayes, K. F. Effects of solution composition and pH on the reductive dechlorination of hexachloroethane by iron sulfide. *Environ. Sci. Technol.* **1998**, *32*, 1276−1284.
(41) Lexa, D.; Saveant, J. M.; Schafer, H. J.; Su, K. B.; Vering, B.; Wang, D. L. Outer-sphere and inner-sphere processes in reductive elimination—Direct and indirect electrochemical reduction of vicinal dibromoalkanes. *J. Am. Chem. Soc.* **1990**, *112*, 6162−6177.
(42) Butler, E. C.; Hayes, K. F. Kinetics of the transformation of trichloroethylene and tetrachloroethylene by iron sulfide. *Environ. Sci. Technol.* **1999**, *33*, 2021−2027.
(43) Schwarzenbach, R. P.; Gschwend, P. M.; Imboden, D. M. *Environmental Organic Chemistry*; John Wiley & Sons: New York, 1993.
(44) Cervini-Silva, J.; Larson, R. A.; Wu, J.; Stucki, J. W. Dechlorination of pentachloroethane by commercial Fe and ferruginous smectite. *Chemosphere* **2002**, *47*, 971−976.
(45) Davenport, A. J.; Oblonsky, L. J. O.; Ryan, H. P.; Toney, M. F. The structure of the passive film that forms on iron aqueous environments. *J. Electrochem. Soc.* **2000**, *147*, 2162−2173.
(46) Ritter, K.; Odziemkowsky, R. W.; Gillham, R. W. An in situ study of the role of surface films on granular iron in the permeable iron wall technology. *J. Contam. Hydrol.* **2004**, *55*, 87−111.
(47) McCormick, M. L.; Adriaens, P. Carbon tetrachloride transformation on the surface of nanoscale biogenic magnetite particles. *Environ. Sci. Technol.* **2004**, *38*, 1045−1053.
(48) Arnold, W. A.; Ball, W. P.; Roberts, A. L. Polychlorinated ethane reaction with zero-valent zinc: Pathways and rate control. *J. Contam. Hydrol.* **1999**, *40*, 183−200.
(49) Scherer, M. M.; Balko, B. A.; Gallagher, D. A.; Tratnyek, P. G. Correlation analysis of rate constants for dechlorination by zero-valent iron. *Environ. Sci. Technol.* **1998**, *32*, 3026−3033.
(50) Totten, L. A. The use of model and probe compounds to investigate the mechanisms of reductive dehalogenation reactions. Ph.D. Dissertation, The Johns Hopkins University, Baltimore, MD, 1999.

Received for review November 8, 2004. Revised manuscript received May 25, 2005. Accepted June 6, 2005.

ES048262E